Energy Conversion and Management 76 (2013) 533–540

Contents lists available at ScienceDirect

Energy Conversion and Management

journal homepage: www.elsevier.com/locate/enconman

Effects of temperature non-uniformity over the heat spreader on the outputs of thermoelectric power generation system

Bimrew Tamrat Admasu, Xiaobing Luo *, Jiawei Yao

School of Energy and Power Engineering, Huazhong University of Science and Technology, Wuhan 430074, China

ARTICLE INFO

Article history:
Received 26 April 2013
Accepted 2 August 2013

Keywords:
Thermoelectricity
Average temperature
Temperature dependent material property
Power
Efficiency

ABSTRACT

Thermal energy from different sources can be converted into electricity by using thermoelectric modules. Controlling the temperature uniformity over the heat spreader of the thermoelectric power generation system is a critical issue for its performance. In this study, we compared the outputs of the thermoelectric power generation system which has uniform temperature distribution with that without uniform temperature distribution over the heat spreader. The model in which thermoelectric materials are temperature related was developed. Finite element based software with thermal–electrical multi-physics coupled was employed to simulate the system. In addition to the simulation, we performed experimental activities. In the simulation and experimental activities, electric current output, power output, open circuit voltage and the efficiency of the system in the cases of uniform and non-uniform temperature distribution over the heat spreader are evaluated. The simulation and experimental results show that the uniform temperature distribution over the heat spreader gives better outputs than the non-uniform temperature distribution.

1. Introduction

The direct conversion of heat energy into electricity, or the reverse, by a semi-conductor thermoelectric power generation devices is related to electron transport phenomena, and the interrelated Seebeck, Petlier and Thomson effects [1,2]. Thermoelectric modules are devices that generate voltage and electrical power by means of temperature difference [3]. They are of great interest in energy applications due to their well-known merits such as the absence of moving components, a reduction of maintenance, and an increase of system life. Its modularity allows for application in a wide scale range without significant losses in performance; the absence of working fluid avoids environmental dangerous leakage [4–8]. They are also direct current (DC) sources and have capability of recovering the huge amount of low grade waste heat [7]. They comprise *p*- and *n-type* semiconductor legs connected thermally in parallel and electrically in series, and sandwiched between two ceramic hot and cold plates [9–12].

Many researchers concerned about the physical properties of thermoelectric material and the manufacturing technique of thermoelectric modules. In addition to the research of thermoelectric material properties, reasonable thermal system design and optimization of thermoelectric generator are equally important for improving the power generation performance. Rodríguez et al. [13] developed a computational model to simulate the thermal and electrical behavior of thermoelectric generators. Their model solves the nonlinear system equations of the thermoelectric and heat transfer. Ahmet and Bekir [14] carried out a theoretical analysis of thermoelectric power generator and they formulated the influence of thermoelectric leg geometry on the device efficiency and power generation. Riffat and Ma [15] performed the geometry optimization of the thermoelectric modules used as generator. Chen et al. [16] and Yu et al. [17] explored the influence of various parameters on the performances including the effect of multiple layers of modules. Xuan et al. [18] employed a phenomenological model to study the effects of internal and/or external interface layers on the thermoelectric devices performance. Crane et al. [11] investigated the characteristics of single-stage, and multi-element thermoelectric generators with the irreversibility of finite-rate heat-transfer, Joulean heat inside the thermoelectric device, and the heat leak through the thermoelectric couple legs. Nuwayhid et al. [19] analyzed the effect of the finite-rate heat transfer between the thermoelectric device and its external heat reservoir on the performance of single-element, and single-stage thermoelectric-generator.

Some researchers used thermoelectric generators in their model as an irreversible heat engine [20]. Gao and Rowe [21], Rowe and Min [22] and Elena et al. [23] investigated the applications of thermoelectric power generation using an industrial waste heat and low temperature waste heat to generate electric power. Some researchers explored the integrated thermoelectric generators in

* Corresponding author. Tel.: +86 13 971460283; fax: +86 27 87557074.
E-mail address: Luoxb@hust.edu.cn (X. Luo).

0196-8904/$ - see front matter © 2013 Elsevier Ltd. All rights reserved.
http://dx.doi.org/10.1016/j.enconman.2013.08.004

Nomenclature

C	specific heat capacity (J kg^{-1} K^{-1})
f	electrical scalar potential (V)
I	electrical current (A)
J	electrical current density (A m^{-2})
N	number of couple legs
P	power (W)
$\dot{q}$	heat generation (W m^{-3})
R	electrical resistivity (Ω m)
R_{pn}	$R_p + R_n$
T	temperature (K)
V	open circuit voltage (V)

Greek symbols

α	Seebeck coefficient (V K^{-1})
α_{pn}	$\alpha_p - \alpha_n$
Δ	change
ε	dielectric permittivity (F m^{-1})
η	system efficiency (%)
λ	thermal conductivity (W m^{-1} K^{-1})
λ_{pn}	$\lambda_p + \lambda_n$
ρ	density (kg m^{-3})
σ	electrical conductivity (S m^{-1})
τ	Thomson coefficient (V K^{-1})

Subscripts

av	average
c	cold junction
ce	ceramic
cu	copper
h	hot junction
n	n-type module leg
p	p-type module leg

Abbreviations

DC	direct current
te	thermoelectric

various micro-reactors and micro-combustors [24,25]. Siddig et al. [26], Chen [27] and Scherrer et al. [28] performed different researches on solar thermoelectric power generation using different system configuration and arrangements.

The conversion efficiency of thermoelectric power generation is mainly restricted by thermoelectric materials. Over the past several years, a number of high power performance thermoelectric materials have been developed [29,30], and some of them are available commercially [31,32]. Sevan et al. [33] investigated the characteristics of a thermoelectric generator at low temperatures. Experimentally, they explored the temperature dependency of Seebeck coefficient and electrical conductivity of a bismuth telluride based thermoelectric generator.

So far, there are so many researches on thermoelectric power generating system, but most of them did not consider the effects of temperature non-uniformity on the outputs of the thermoelectric power generation system. The purpose of the present study is to realize this. The study compares the outputs of thermoelectric system when the input temperature is uniformly distributed over the heat spreader with non-uniform temperature distribution case. The analysis model considers the temperature dependency of all the important thermoelectric material properties. The second and third sections of this study introduce the governing equations and finite element modeling of thermoelectricity, respectively. The fourth section introduces the boundary conditions. The fifth section introduces the material properties. The sixth section introduces the mesh independency of the thermoelectric power generation system. The seventh section introduces the results and the discussion part. The final part presents the conclusion part of this paper.

2. Governing equations of thermoelectricity

The general heat conduction and continuity equations of electric charge for the thermoelectric analysis can be expressed as [34–36]:

$$\rho C\frac{\partial T}{\partial t}+\nabla\cdot(T[\alpha]\cdot J)-\nabla\cdot([\lambda]\cdot\nabla T)=\dot{q}, \tag{1}$$

$$\nabla\cdot\left([\varepsilon]\cdot\nabla\frac{\partial f}{\partial t}\right)+\nabla\cdot([\sigma]\cdot[\alpha]\cdot\nabla T)+\nabla\cdot([\sigma]\cdot\nabla f)=0 \tag{2}$$

where ρ, C, T, J, f and $\dot{q}$ are the density, specific heat capacity, absolute temperature, electric current density vector, electric scalar potential, and heat generation rate per unit volume, respectively. $[\lambda]$ is the thermal conductivity matrix, $[\sigma]$ is the electric conductivity matrix, $[\alpha]$ is the Seebeck coefficient matrix, and $[\varepsilon]$ is the dielectric permittivity matrix.

In a steady state thermoelectric analysis, thermal and electrical loads do not vary over time. In the present steady-state model, material properties of all components are considered to be an isotropic. The coupled equations of thermoelectricity can be written as follows:

$$\nabla\cdot(\sigma\alpha\nabla T)+\nabla\cdot(\sigma\nabla f)=0 \tag{3}$$

$$\nabla\cdot(T\alpha J)-\nabla\cdot(\lambda\nabla T)=\dot{q} \tag{4}$$

The heat generation rate, $\dot{q}$ is expressed by [37]

$$\dot{q}=J\cdot\alpha\nabla T-\nabla\cdot(\lambda\nabla T)+\tau J\cdot\nabla T \tag{5}$$

where τ is the Thomson coefficient and it can be expressed as follows

$$\tau=T\frac{d\alpha}{dT} \tag{6}$$

Keeping the non-ohmic current voltage relation in both legs of the devices in mind, the governing equations of the electrical field inside a control volume under steady state can be written as [4]

$$(\nabla V)_p=-\alpha_p(T_p)\nabla T_p-R_p(T_p)J \tag{7}$$

$$(\nabla V)_n=-\alpha_n(T_n)\nabla T_n-R_n(T_n)J \tag{8}$$

The first terms in the right side of Eqs. (7) and (8) are the Seebeck electromotive force (EMF) increase due to the temperature gradient, and the second terms are the voltage drop due to the current flowing through the control volume.

3. Finite element modeling

Fig. 1 shows the finite element model of the thermoelectric power generation system. Here, material selections, meshing and boundary conditions for the model were set. The thermo-electric analysis option within the ANSYS Workbench was used to

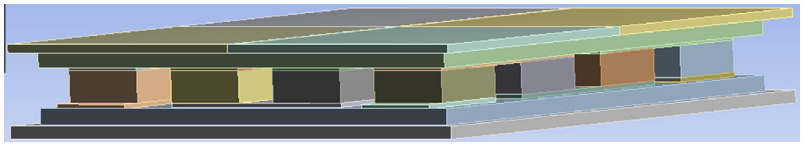

Fig. 1. Finite element model of thermoelectric power generation system.

represent the bismuth telluride as thermoelectric couple legs material. The heat spreader, dielectric ceramic cover and the heat sink, which are the other components of the thermoelectric power generation system, included in the modeled as thermal masses with isotropic thermal conductivity and electrical resistivity.

4. Boundary conditions

The study set different boundary conditions to simulate the research model. The input temperature over the heat spreader was variable while the heat sink temperature was an average ambient temperature of 298 K. The free surfaces of the heat spreader and the heat sink were exposed to the surrounding air and heat might be removed from the surfaces due to natural convection. The film coefficient for these surfaces assumed to be 25 $W/(m^2\,K)$ at an average ambient temperature. The free surfaces of the thermoelectric legs, the connectors and the dielectric ceramic covers were insulated and had an almost zero film coefficient that is $1 \times 10^{-8}\,W/(m^2\,K)$ at an average ambient temperature. Initially, a DC voltage of 0 V (electrically grounded) and 0.0006 V set for the low potential and the high potential boundary conditions, respectively.

5. Material properties

The selection of thermoelectric materials directly affects the performance of the thermoelectric device. The study used bismuth telluride as material of thermoelectric module legs. The properties of this material such as the Seebeck coefficient, thermal conductivity and electrical conductivity all depend on temperature. The physical properties of the thermoelectric module legs provided by Melcor [38] were used for this simulation and shown as follows

$$\alpha_{pn} = (22224 + 930.6T_{av} - 0.9905T_{av}^2) \times 10^{-9}\ (V/K) \quad (9)$$

$$R_{pn} = (5112 + 163.4T_{av} + 0.6279T_{av}^2) \times 10^{-10}\ (\Omega\,m) \quad (10)$$

$$\lambda_{pn} = (62,605 - 277.7T_{av} + 0.4131T_{av}^2) \times 10^{-4}\ (W/(m\,K)) \quad (11)$$

where $T_{av} = (Th + Tc)/2$ is the mean temperature of the hot and cold junctions.

The material type of the connectors, heat spreader and the heat sink for this simulation was copper. The physical properties of copper and ceramic at an average temperature of 400 K are shown in Table 1.

6. Mesh independency

The study performed a mesh sensitivity analysis for the thermoelectric power generation system to check its mesh independency. The default method for meshing that is rectangular mesh, which is shown in Fig. 2. The study prepared three models to check the mesh sensitivity and the mesh size was progressively refined. The first model had 37,760 nodes and 4959 elements with element size of 9×10^{-4} m, and yields a current output of 5.6077 A, the second model had 41,136 nodes and 5427 elements with element size of 8.5×10^{-4} m, and yields a current output of 5.6034 A, and the third model had 44,542 nodes and 5890 elements with a mesh size of 8×10^{-4} m, and yields a current output of 5.6017 A. Finally, the study confirmed that as the mesh size refines more, the current output does not have obvious change.

Table 1
Physical properties of copper and ceramic.

Physical properties	Units	Copper	Ceramic	References
λ	W/(m K)	398	25.12	[39]
R	Ω m	1.67×10^{-8}	5.03×10^{10}	[39]

7. Results and discussion

7.1. Numerical simulation

The performance of thermoelectric power generation system might be negatively affected by different factors, such as losses due to thermal resistance of the components, losses due to thermal contact and electrical contact resistances at the interfaces between the components, and temperature non-uniformity on the heat spreader. All the above losses are due to the geometry of the thermoelectric power generation system. In the present paper, we focused on the effect of temperature non-uniformity. As seen from the finite element model in Fig. 1, the heat spreader was divided into four partitions. In the first case that is the uniform temperature distribution, the study used the same temperature values for the four partitions and the outputs were evaluated for different temperature ranges. In the second case that is the non-uniform temperature distribution, the study used different temperature values at the four partitions but an equal-average temperature with that of the case of the uniform temperature distribution at each step. The other inputs were the geometry data, the boundary conditions and temperature dependent thermoelectric material properties such as the Seebeck coefficient, thermal conductivity and electrical resistivity.

Figs. 3 and 4 show the simulation results of the temperature contour in the cases of uniform and non-uniform temperature distribution over the heat spreader. The sample temperature data taken to simulate in the case of uniform temperature distribution were 360.75 K, 370.75 K, 380.75 K, 390.75 K, 400.75 K, 410.75 K, 420.75 K and 430.75 K and the temperature data in the case of non-uniform temperature distribution were (435 K, 360 K, 350 K and 298 K), (435 K, 380 K, 370 K and 298 K), (435 K, 400 K, 390 K and 298 K), (435 K, 420 K, 410 K and 298 K), (435 K, 440 K, 430 K and 298 K), (435 K, 460 K, 450 K and 298 K), (435 K, 480 K, 470 K and 298 K) and (435 K, 500 K, 490 K and 298 K). The average temperature of the non-uniform temperature distribution at each step was equal with that of the uniform temperature distribution. For example, the first input temperature data in the case of uniform temperature distribution that is 360.75 K is equal with the average temperature of the first input temperature data of the non-uniform temperature distribution that is (435 K, 360 K, 350 K and 298 K).

The hot junctions of all the thermoelectric module couple legs are inter-connected by thermal conductive copper strips. When we see the assembly of the system, all the conductive copper strips are inter-connected with the upper and lower dielectric ceramic

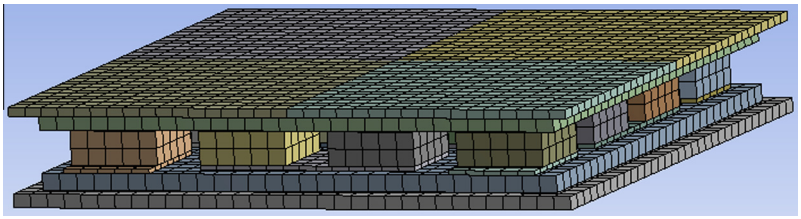

Fig. 2. Mesh model of thermoelectric power generation system with rectangular elements.

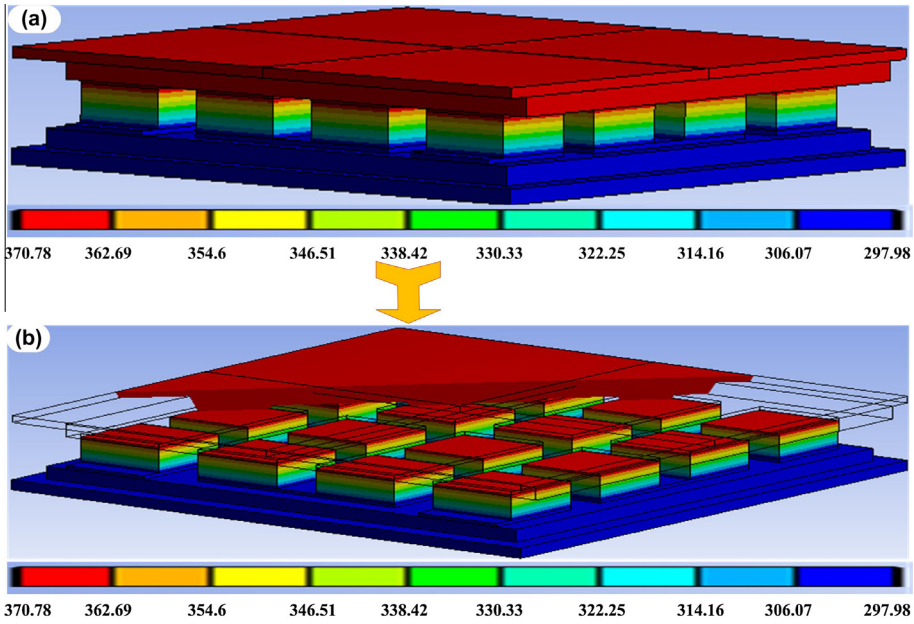

Fig. 3. Simulation result of temperature contour in the case of uniform input temperature of 370.75 K.

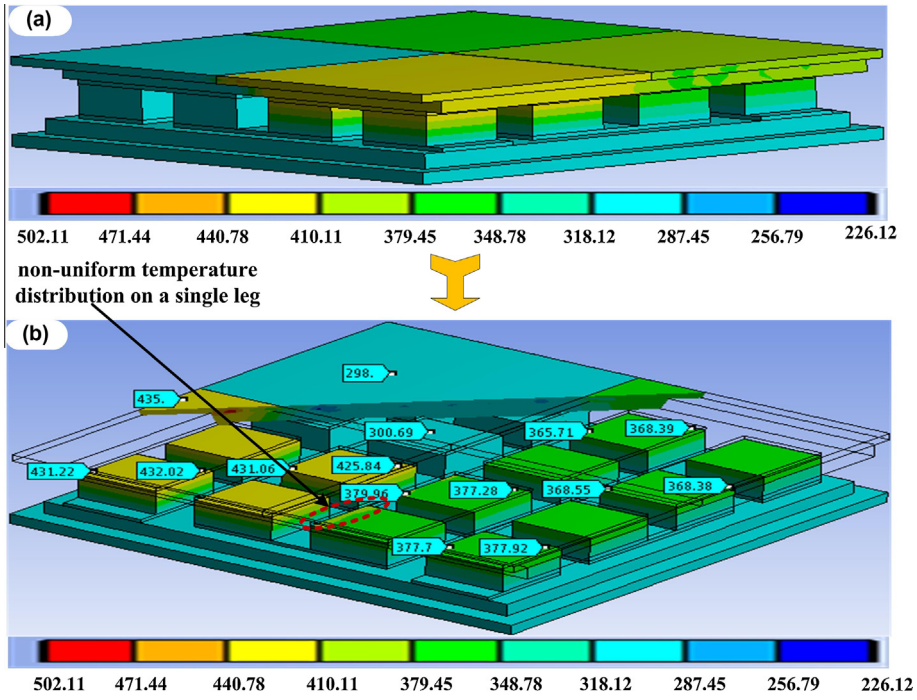

Fig. 4. Simulation result of temperature contour in the case of non-uniform input temperature of (435 K, 380 K, 370 K and 298 K).

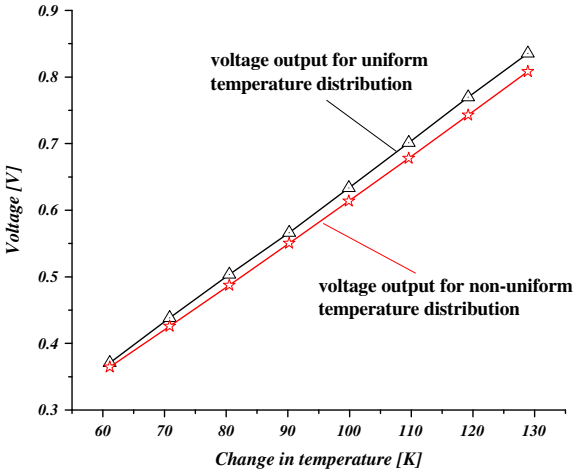

Fig. 5. Voltage output versus the temperature change between the junctions in the cases of uniform and non-uniform temperature distribution over the heat spreader.

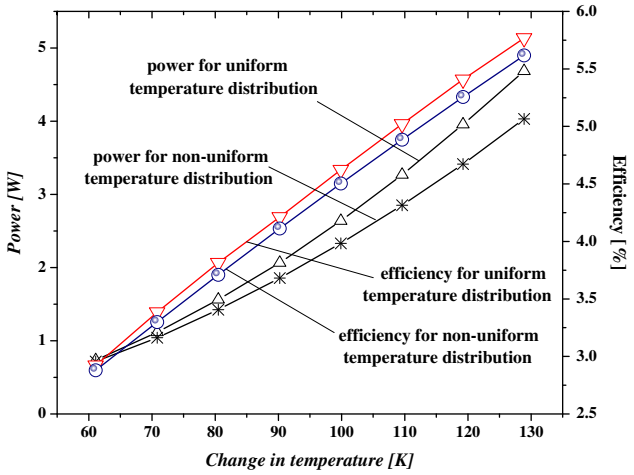

Fig. 8. Power output and system efficiency versus the temperature change between the junctions in the cases of uniform and non-uniform temperature distribution over the heat spreader.

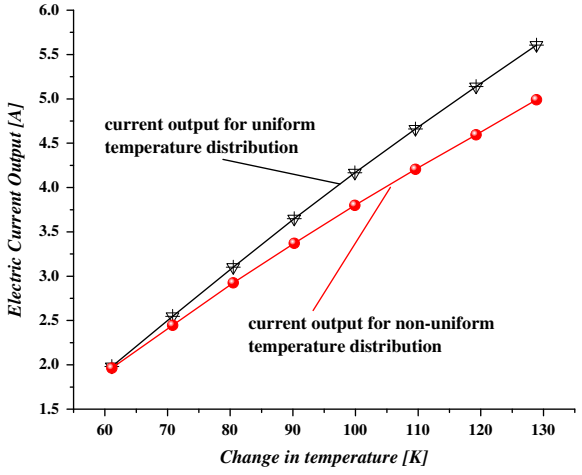

Fig. 6. Electric current output versus the temperature change between the junctions in the cases of uniform and non-uniform temperature distribution over the heat spreader.

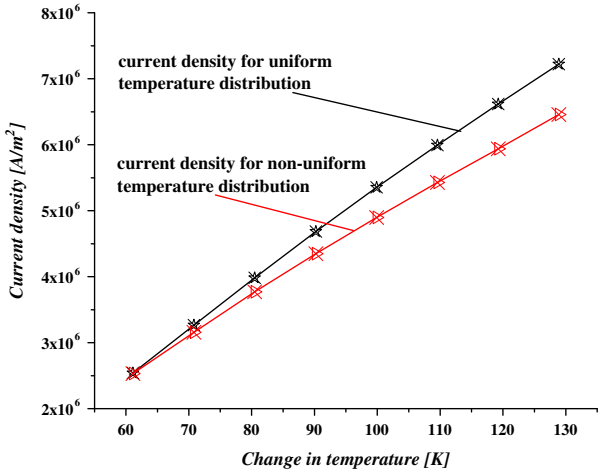

Fig. 7. Electric current density versus the temperature change between the junctions in the cases of uniform and non-uniform temperature distribution over the heat spreader.

cover which have direct contact with the heat spreader and heat sink, respectively. One can see from the temperature contour of Fig. 4a and b, in the case of non-uniform temperature distribution, on a single system, the hot junction of all the module legs have different temperature values. As seen in Fig. 4b, even on a single module leg, at different coordinates, the temperature distribution is non-uniform. As an example, on a single module leg, the hot junction temperature values at different coordinates are 431.06 K and 425.84 K. One can see from Fig. 4 that some parts of the heat spreader have lower temperature values than some parts of the module legs hot junction temperature values. So, due to the second law of thermodynamics, heat might be flowed from the hot junction of the module legs to the heat spreader which is in the reverse direction. If the temperature distribution on the heat spreader is uniform, as seen in Fig. 3a and b, heat will be flowed only from the heat spreader to the hot junction of the module legs.

The junctions' temperature cannot be determined simply from the input temperature on the heat spreader due to the thermoelectric effect inside the thermoelectric module legs. Those thermoelectric effects are, the internal irreversibility caused by Joulean electrical resistivity loss, heat conduction loss through the semiconductor legs between the hot and cold junctions, Peltier effect at the hot and cold junctions, and a reversible absorption or liberation of heat in a homogenous temperature and electrical gradient for temperature dependent thermoelectric materials due to Thomson effect. So, reading the temperature from the simulation result at the junctions was indispensable.

To simulate the system for an open circuit voltage, low potential boundary condition was set on the external face of conductive copper strip that connects the external electrical load and the n-leg, and the high potential boundary condition was set on the external face of the conductive copper strip that connects the external electrical load and the p-leg.

Fig. 5 shows the thermoelectric power generation system voltage output versus the change in temperature between the junctions in the cases of uniform and non-uniform temperature distribution over the heat spreader. It can be seen that the voltage output is linear and increasing function of the change in junctions' temperature. The linear relationship is approximate because there are factors like temperature dependent thermoelectric material properties and radiative heat transfer which caused non-linearity. As seen from Fig. 5, when the temperature change between the hot and cold junctions increases, the voltage outputs in both cases increase but the increment in the case of uniform temperature

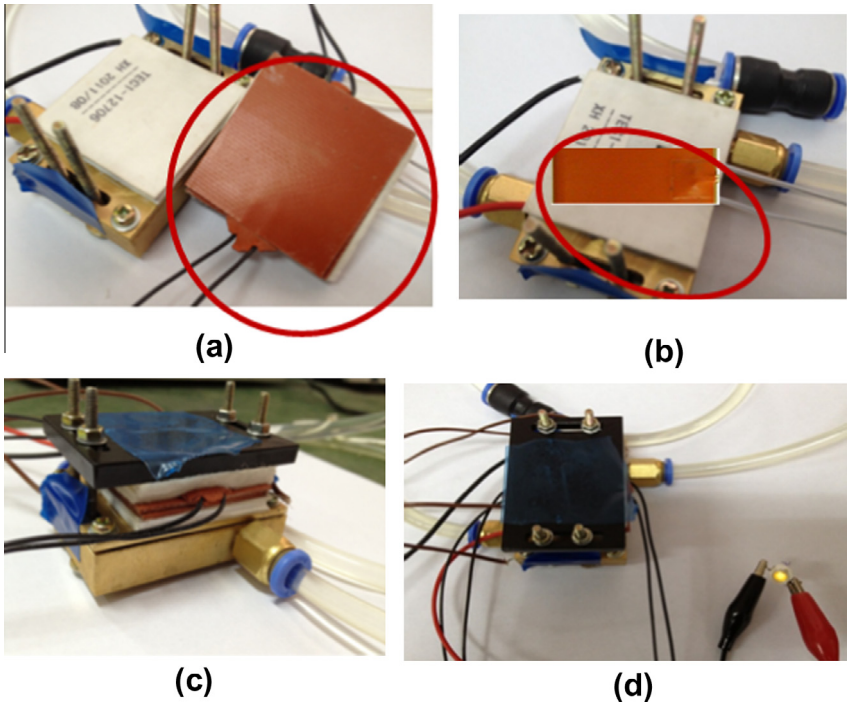

Fig. 9. Experimental components and setup (a) the heater covered all top surface of the module, (b) the heater covered some parts of the module, (c) and (d) experiment set up in case (a) and case (b), respectively.

distribution is relatively higher. We can see from Fig. 5 that when the temperature change is 90 K, the voltage outputs in the cases of uniform and non-uniform temperature distribution over the heat spreader are 0.567 V and 0.55 V, respectively and the voltage difference between the two cases is 0.017 V. When the temperature change is 128 K, the voltage output in the cases of uniform and non-uniform temperature distribution are 0.84 V and 0.81 V, respectively and the voltage difference between the two cases is 0.03 V.

The electric current generated has direct relationship with the open circuit voltage. Based on the Seebeck effect, and the temperature difference between the hot and cold junctions, causes an electric current to flow in the circuit. Fig. 6 shows the electric current output versus the temperature change between the junctions in the cases of uniform and non-uniform temperature distribution over the heat spreader. As seen from the figure, when the temperature change between the hot and cold junctions increases, the electrons on the hotter side vibrates more vigorously so they tend to move towards the colder side where the electrons are moving more slowly and the current generation will increase. From Fig. 6, one can see that the electric current is parabolic-like and increasing function of the temperature change between the hot and cold junctions in both uniform and non-uniform temperature cases. Actually, the current output and temperature have linear relationships but there are factors like temperature dependence of thermoelectric material properties and radiative heat transfer to cause the non-linearity. As mentioned in the previous section, due to the second law of thermodynamics, the current output is relatively higher in the case of uniform temperature distribution over the heat spreader than an equal average non-uniform temperature distribution. Fig. 7 shows the electric current density versus the change in temperature between the junctions in the cases of uniform and non-uniform temperature distribution over the heat spreader. It has the same profile with that of the electric current output because all the parameters influence the current density. As the temperature gradient increases, the electric current density increases parabolic-like. As seen from the figure, if we keep the temperature distribution uniform over the heat spreader, we can get better particle flow.

The electric power output can be evaluated from the heat input at the hot junction and the heat dissipated from the thermoelectric module through the heat sink and the efficiency of the system can be evaluated from the ratio of electric power output to the heat input at the hot junction of the thermoelectric module. Fig. 8 shows the power output and system efficiency versus the temperature change between the junctions in the cases of uniform and non-uniform temperature distribution over the heat spreader. It can be seen that the power output and efficiency are parabolic-like and increasing function of the change in temperature between the hot and cold junctions in both cases that is the uniform and non-uniform temperature distribution over the heat spreader. The power output and system efficiency increment in the case of uniform temperature distribution are relatively higher. One can see from Fig. 8 that when the change in temperature is 80.5 K, the power output and system efficiency are 1.562 W and 3.81% in the case of uniform temperature distribution and 1.425 W and 3.71% in the case of non-uniform temperature distribution, respectively. The differences in power output and system efficiency at this point between the two cases are 0.137 W and 0.1%, respectively. When the change in temperature is 129 K, the power output and system efficiency are 4.68 W and 5.77% in the case of uniform temperature distribution and 4.032 W and 5.62% in the case of non-uniform temperature distribution, respectively. The differences in power output and system efficiency at this point between the two cases are 0.648 W and 0.15%, respectively.

7.2. Experimental validation

The commercial thermoelectric module TEC1-12706 type and the resistance wire silicon rubber heater TY-SRH were tightly clamped between the upper frame and the circulating water reservoir. The silicon rubber heater glued to the module using epoxy

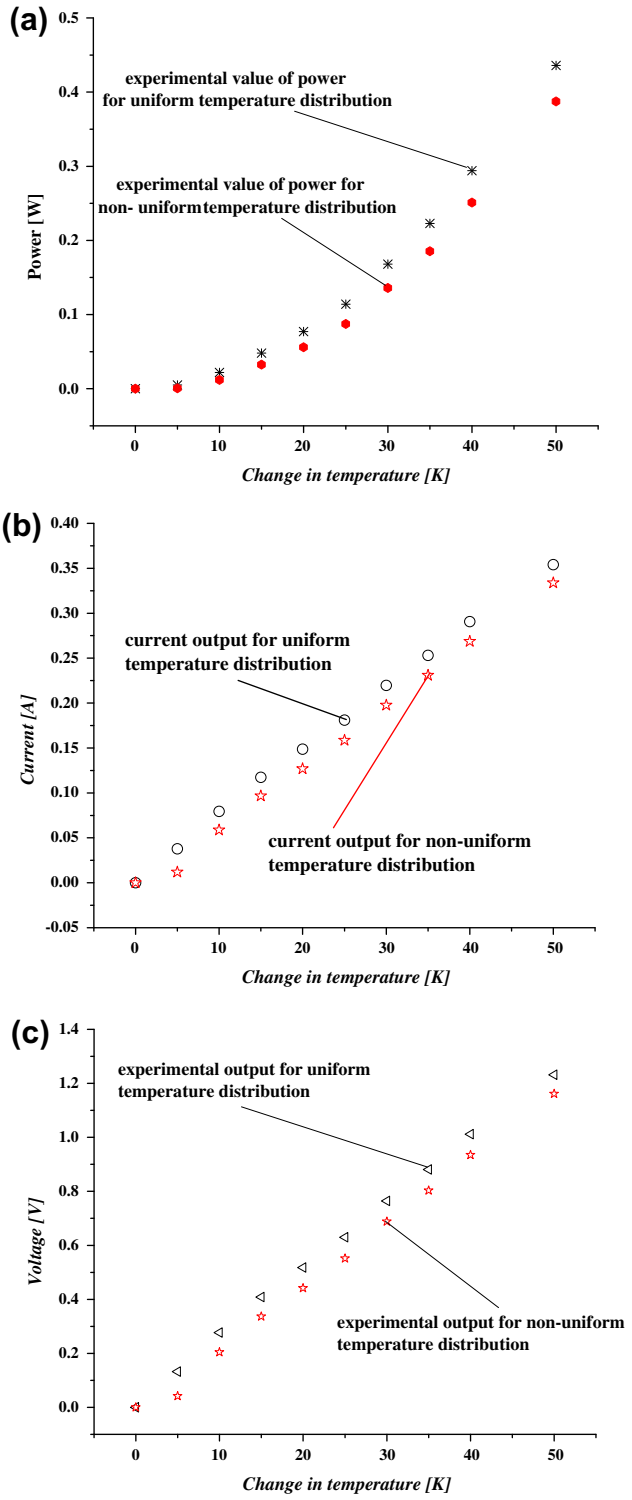

Fig. 10. Experimental results: (a) Power generated in the case of uniform and non-uniform temperature distribution versus the temperature change between the hot and cold surfaces of the thermoelectric module, (b) electric current generated in the case of uniform and non-uniform temperature distribution versus the temperature change between the hot and cold surfaces of the thermoelectric module, and (c) voltage output in the case of uniform and non-temperature distribution versus the temperature change between the hot and cold surfaces of the thermoelectric module.

resin materials. The two lead wires from the resistance heater connected to an external power supply. Measuring equipments like data acquisition system and digital multimeter were used. From the data acquisition multimeter, "K" type thermocouples were used to measure the temperatures of heat sink, the hot and cold surfaces of the thermoelectric module, the heater and the ambient.

The Circulating water used for heat sink had a maximum flow rate of 8.3 L min^{-1} and a maximum head of 0.8 m. The study used two different sample sizes of silicon rubber heaters. The first sample covered the whole upper surface of the thermoelectric module as seen from Fig. 9a which has the same size with the thermoelectric module, 40 mm by 40 mm and delivers uniform temperature distribution. As seen from Fig. 9b, the second sample size was 15 mm by 40 mm and covered and heat up some part of the upper surface of the thermoelectric module. When the experiment performed, we used the insulating material (i.e. asbestos) to cover the surroundings of the heater and the uncovered parts of the module.

In the experiment, the parameters for the two cases were the same only the coverage of the heater. When we performed the experiment, we connected an external electrical load of 1.5 Ω. Fig. 10 shows the experimental results on the effect of temperature non-uniformity over the heat spreader. As seen from the figure, if we keep the temperature distribution uniform over the hot surface of the thermoelectric module, we can get better output.

8. Conclusion

In this paper, we formulated the governing equations of thermoelectricity and conducted finite element modeling and analysis to compare the effect of uniform and an equal average non-uniform temperature distribution on the output of thermoelectric power generation system. The experimental and simulation results show that maintaining the temperature distribution uniform all over the top surface of the heat spreader of the thermoelectric power generation system delivers better outputs.

References

[1] Rowe DM. CRC handbook of thermoelectric. 1st ed. Boca Raton: CRC Press; 1995.
[2] Bejan A. Advanced engineering thermodynamics, 3rd ed. Hoboken, NJ; 2006.
[3] Chen M, Lasse AR, Thomas JC, John KP. Numerical modeling of thermoelectric generators with varying material properties in a circuit simulator. IEEE Trans Energy Convers 2009;24.
[4] Chen M, Lasse AR, Thomas C. A three-dimensional numerical model of thermoelectric generators in fluid power systems. Int J Heat Mass Transfer 2011;54:345–55.
[5] Omer SA, Infield DG. Design optimization of thermoelectric devices for solar power generation. Solar Energy Mater Solar Cells 1998;53:67–82.
[6] Arunkumar P, Arunprakash K, Rajarajan P, Balaji G, Saravanan VA. High efficient renewable power generation using bi-conical flask technology. 2nd International conference on environmental science and technology IPCBEE, © (2011), vol. 6. Singapore: IACSIT Press; 2011.
[7] Gou X, Xiao H, Yang S. Modeling, experimental study and optimization on low-temperature waste heat thermoelectric generator system. Appl Energy 2010;87:3131–6.
[8] Atik K. Numerical simulation of a solar thermoelectric generator. Energy Sources, Part A 2011;33:760–7.
[9] Rowe DM. General principles and basic considerations. In: Thermoelectrics handbook: macro to nano. Boca Raton, FL, USA: CRC Press; 2006.
[10] Yamanashi M. A new approach to optimum design in thermoelectric cooling systems. J Appl Phys 1996;80.
[11] Crane DT, Jackson SG. Optimization of cross flow heat exchangers for thermoelectric waste heat recovery. Energy Convers Manage 2004;45:1565–82.
[12] Riffat SB, Ma Xiaoli. Improving the coefficient of performance of thermoelectric cooling systems: a review. J Energy Res 2004;28:753–68.
[13] Rodríguez A, Vián JG, Astrain D, Martínez A. Study of thermoelectric systems applied to electric power generation. Energy Convers Manage 2009;50:1236–43.
[14] Ahmet ZS, Bekir SY. The thermoelement as thermoelectric power generator: effect of leg geometry on the efficiency and power generation. Energy Convers Manage 2013;65:26–32.
[15] Riffat SB, Ma X. Optimum selection (design) of thermoelectric modules for large capacity heat pump applications. Int J Energy Res 2004;28:1231–42.
[16] Chen L, Li J, Sun F, Wu C. Performance optimization of a two-stage semiconductor thermoelectric-generator. Appl Energy 2005;82:300–12.

[17] Yu J, Zhao H, Xie K. Analysis of optimum configuration of two-stage thermoelectric modules. Cryogenics 2007;47:89–93.
[18] Xuan XC, Ng KC, Yap C, Chua HT. A general model for studying effects of interface layers on thermoelectric devices performance. Int J Heat Mass Transfer 2002;45:5159–70.
[19] Nuwayhid RY, Shihadeh A, Ghaddar N. Development and testing of a domestic woodstove thermoelectric generator with natural convection cooling. Energy Convers Manage 2005;46:1631–43.
[20] Ozkaynak S, Gotkun S. Effect of irreversibilities on the performance of a thermoelectric generator. Energy Convers Manage 1994;35(12):1117–21.
[21] Gao M, Rowe DM. Optimization of thermoelectric module geometry for "waste" heat electric power generation. J Power Sources 1992;38:253–9.
[22] Rowe DM, Min G. Evaluation of thermoelectric modules for power generation. J Power Sources 1998;73:193–8.
[23] Elena OV, Enescu D, Ionel M, Mihail FS. Numerical simulation of thermoelectric system, latest trends on systems, vol. ii.
[24] Yoshida K, Tanaka S, Tomonari S, Satoh D, Esashi M. High-energy density miniature thermoelectric generator using catalytic combustion. IEEE/ASME, J Microelectromech Syst 2006;15:195–203.
[25] Federici JA, Norton DG, Bruggemanna T, Voit KW, Wetzel ED, Vlachos DG. Catalytic micro combustors with integrated thermoelectric elements for portable power production. J Power Sources 2006;161:1469–78.
[26] Siddig AO, David G. Infield, design and thermal analysis of a two stage solar concentrator for combined heat and thermoelectric power generation. Energy Convers Manage 2000;41:737–56.
[27] Chen J. Thermodynamic analysis of a solar driven thermoelectric generator. J Appl Phys 1996;79.
[28] Scherrer H, Vikhor L, Lenoir B, Dauscher A, Poinas P. Solar thermoelectric generator based on Skutterudites. J Power Sources 2003;115:141–8.
[29] Chen G, Dresselhaus MS, Dresselhaus G, Fleurial JP, Caillat T. Recent developments in thermoelectric materials. Int Mater Rev 2003;48:1–25.
[30] Sootsman JR, Duck YC, Kanatzidis MG. New and old concepts in thermoelectric materials. Angew Chem Int Ed Engl 2009;48:8616–39.
[31] Poudel B, Hao Q, Ma Y, Lan Y, Minnich A, Yu B. High-thermoelectric performance of nanostructured bismuth antimony telluride bulk alloys. Science 2008;320:634–8.
[32] Zhao XB, Ji XH, Zhang YH, Zhu TJ, Tu JP, Zhang XB. Bismuth telluride nanotubes and the effects on the thermoelectric properties of nanotube-containing nanocomposites. Appl Phys Lett 2005;86:06211.
[33] Sevan K, Altug S, Fatih ZO, Turker S. Characterization of a thermoelectric generator at low temperatures. Energy Convers Manage 2012;62:47–50.
[34] Harman TC, Honig JM. Thermoelectric and thermo magnetic effects and applications. New York: McGraw-Hill; 1967.
[35] Callen HB. Thermodynamics; an introduction to the physical theories of equilibrium thermostatics and irreversible thermodynamics. New York: Wiley; 1960.
[36] Antonova EE, Looman DC. In: 24th International conference on thermoelectrics (ICT); 2005. p. 197–200.
[37] HoSung L. The Thomson effect and the ideal equation on thermoelectric coolers. Energy 2013;56:61–9.
[38] Melcor. Thermoelectric handbook. <http://www.melcor.com/formula.htm>.
[39] James FS, William A. Material science and engineering handbook. third ed. LLC: CRC Press; 2001.